NANO LETTERS

Letter

pubs.acs.org/NanoLett

Cost-Effective, Transfer-Free, Flexible Resistive Random Access Memory Using Laser-Scribed Reduced Graphene Oxide Patterning Technology

He Tian,[†,†] Hong-Yu Chen,[‡,†] Tian-Ling Ren,[†,*] Cheng Li,[†] Qing-Tang Xue,[†] Mohammad Ali Mohammad,[†] Can Wu,[†] Yi Yang,[†] and H.-S Philip Wong[‡,*]

[†]Institute of Microelectronics and Tsinghua National Laboratory for Information Science and Technology (TNList), Tsinghua University, Beijing 100084, China

[‡]Department of Electrical Engineering and Center for Integrated Systems, Stanford University, Stanford, California 94305, United States

Supporting Information

ABSTRACT: Laser scribing is an attractive reduced graphene oxide (rGO) growth and patterning technology because the process is low-cost, time-efficient, transfer-free, and flexible. Various laser-scribed rGO (LSG) components such as capacitors, gas sensors, and strain sensors have been demonstrated. However, obstacles remain toward practical application of the technology where all the components of a system are fabricated using laser scribing. Memory components, if developed, will substantially broaden the application space of low-cost, flexible electronic systems. For the first time, a low-cost approach to fabricate resistive random access memory (ReRAM) using laser-scribed rGO as the bottom electrode is experimentally demonstrated. The one-step laser scribing technology allows transfer-free rGO synthesis directly on flexible substrates or non-flat substrates. Using this time-efficient laser-scribing technology, the patterning of a memory-array area up to 100 cm^2 can be completed in 25 min. Without requiring the photoresist coating for lithography, the surface of patterned rGO remains as clean as its pristine state. Ag/HfO_x/LSG ReRAM using laser-scribing technology is fabricated in this work. Comprehensive electrical characteristics are presented including forming-free behavior, stable switching, reasonable reliability performance and potential for 2-bit storage per memory cell. The results suggest that laser-scribing technology can potentially produce more cost-effective and time-effective rGO-based circuits and systems for practical applications.

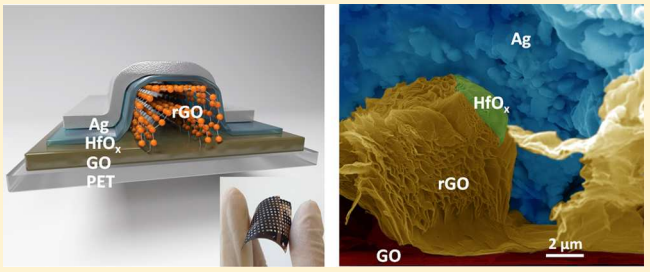

Graphene has received much attention due to its single-atom layer thickness with superior properties[1] such as ultrahigh mobility, room temperature quantum hall effect, ultrahigh thermal conductivity, and transparency. In order to employ graphene for practical applications,[2] the first step is the realization of efficient fabrication and transfer processes to obtain large-area graphene films on desired substrates. A lot of effort has been made for the fabrication and transfer process previously. A representative work is the application of roll-to-roll production of 30-in. graphene films for transparent electrodes.[3] Recently, Jaechul Ryu et al.[4] have demonstrated a rapid thermal chemical vapor deposition (CVD) method, which allows graphene growth over 400 × 300 mm^2 area in less than 1 h. The face-to-face transfer method has demonstrated the transfer of 8-in. wafer-scale graphene onto silicon substrate successfully.[5] However, the problems caused by the graphene patterning process still remain, such as photoresist contamination, film cracking, etc.[6,7] Moreover, the zero band gap of graphene limits its applications in low power electronics.

Reduced graphene oxide (rGO) is a kind of graphene derivative with the advantages of an open band gap and rapid, large-scale production.[8] Thinner rGO exhibits graphene-like ambipolar transistor characteristics, while thicker films behave as graphite-like semimetals.[9] Resonators fabricated with rGO have figures of merit potentially exceeding those of pure graphene resonators.[10] Laser-scribing technology[11] is a good solution to realize simultaneously direct growth and patterning of rGO. It is a low-cost, time-efficient, and maskless flexible fabrication process. Various laser-scribed rGO (LSG) components such as capacitors,[12] gas sensors,[13] strain sensors,[14] and multifunctional devices[15] have been demonstrated. Developing memory modules using laser-scribing technology could broaden system-level applications. Resistive random access memory (ReRAM) is a promising candidate for next generation nonvolatile memory.[16] Among the most commonly reported ReRAM are those whose switching mechanism is based on the formation of cation filaments (cation-based ReRAM),[17] and those based on the formation of oxygen vacancies (oxide-based ReRAM).[18] The

Received: February 14, 2014
Revised: May 1, 2014
Published: May 6, 2014

   dx.doi.org/10.1021/nl5005916 | *Nano Lett.* 2014, 14, 3214−3219

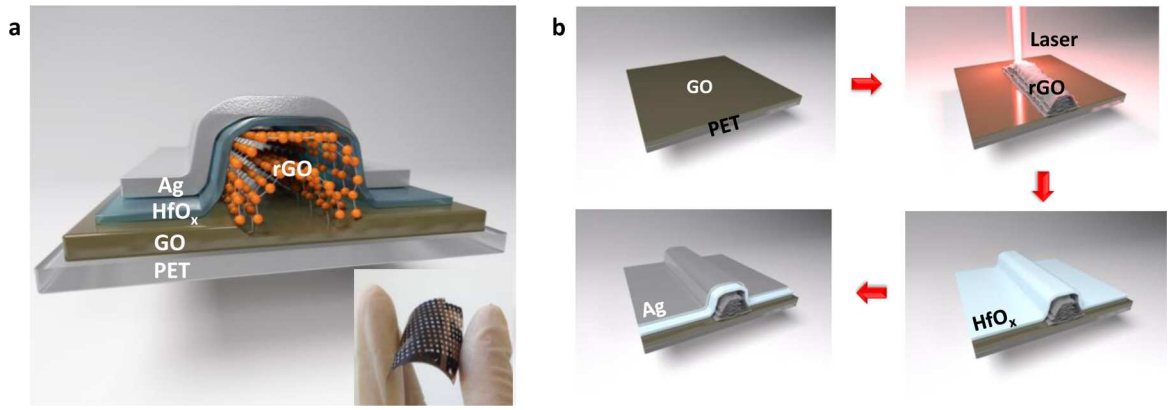

Figure 1. Device structure and process flow of the LSG-ReRAM. (a) Device structure of the LSG-ReRAM. Inset: The photo of the fabricated LSG-ReRAM on a PET substrate. (b) Diagrams showing the main fabrication processing steps of the LSG-ReRAM.

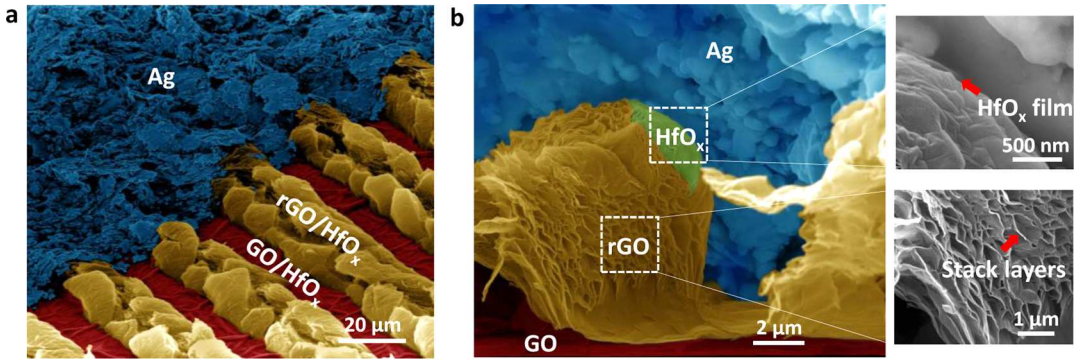

Figure 2. Morphology of the LSG-ReRAM. (a) Top view SEM image of the LSG-ReRAM in false color. The thickness of HfO_x is 10 nm. The height of the rGO line is 10 μm. (b) Cross-sectional view SEM image of the LSG-ReRAM. The insets highlight the HfO_x thin film and stacked rGO layers, respectively.

forming process for the oxide-based ReRAM is considered to be dielectric soft breakdown. For practical applications, it is desirable to make the so-called "forming-free" devices, which actually have a forming voltage comparable to the devices' SET voltages.[18] It is reported that ReRAM provides better electrical characteristics compared to Flash in terms of programming voltages, switching speed and reliability. Furthermore, scalability[19] down to 10 × 10 nm^2 and cost-effective 3D integration potential[20,21] have also been demonstrated in the research field of ReRAM. Previously, graphene-based memory[22−25] was fabricated based on the CVD method, which required a few hours from material synthesis in CVD, to transferring graphene onto desire substrates, and finally to patterning it into desired shapes. Moreover, all the reported graphene memory devices[22−25] were fabricated on rigid substrates.

For the first time, a low-cost, transfer-free, flexible ReRAM based on LSG (LSG-ReRAM) is experimentally demonstrated. The fabricated Ag/HfO_x/LSG structure exhibits forming-free behavior and stable switching up to 100 cycles. Moreover, the reasonable reliability performance and 2-bit storage capability are demonstrated. Three kinds of top electrode materials (Ag, Pt and LSG) are employed to investigate the conducting mechanism of the LSG-ReRAMs. The temperature-dependent electrical measurement of the LSG-ReRAM further sheds light on the working principles of the LSG-ReRAM.

Results. *Fabrication of the LSG-ReRAM.* A maskless and programmable laser-scribing technology is used to realize low-cost laser scribed rGO (LSG) production on flexible substrates. This laser-scribing technology enables precise patterning of rGO over a large area. For example, 100 cm^2 of patterned rGO can be obtained in ~25 min, corresponding to 4 × 10^6 μm^2/min. The details of fabricating LSG are described in the Methods. The structure of the fabricated LSG-ReRAM is shown in Figure 1a. The LSG-ReRAM is formed of a sandwich of Ag/HfO_x/LSG layers. It is noted that the detailed microstructure of the LSG-ReRAM is entirely different from a conventional planar structure for the ReRAM. The thickness of the original graphene oxide (GO) film on Polythylene terephthalate (PET) is 1 μm. After the LSG is formed, the surface is raised due to the rapid loss of oxygen.[11] As a result, the LSG-ReRAM has an exaggerated topography as visualized in Figure 1a. The main process flow of the LSG-ReRAM is shown in Figure 1b.

Morphology of the LSG-ReRAM. The SEM morphology and structure are shown in false colors (Figure 2a). The Ag top electrode is colored blue. The bottom GO is identified in red according to its distinct texture. After the laser scribing, the GO was reduced into rGO by the laser pulses. The swollen 20 μm wide lines of the LSG are clearly identifiable on the GO substrate. The cross-sectional SEM image further confirms the presence of the 10 μm thick LSG (See Supporting Information Figure S1). The LSG is 10 times thicker than the original GO film. The optical image of the LSG is shown in Figure S2. Raman spectrum (Figure S3) confirms that the LSG is a multilayer rGO stack. In the comparison with GO, it is noticed that oxygen is reduced significantly in rGO (Figure S4). The cross-sectional view of LSG-ReRAM, formed of Ag/HfO_x/LSG 3D structure, is shown in Figure 2b. The Ag particles of around 1 μm are clearly identified in the main SEM image. Contrarily, the 10 nm-HfO_x

dx.doi.org/10.1021/nl5005916 | *Nano Lett.* 2014, 14, 3214−3219

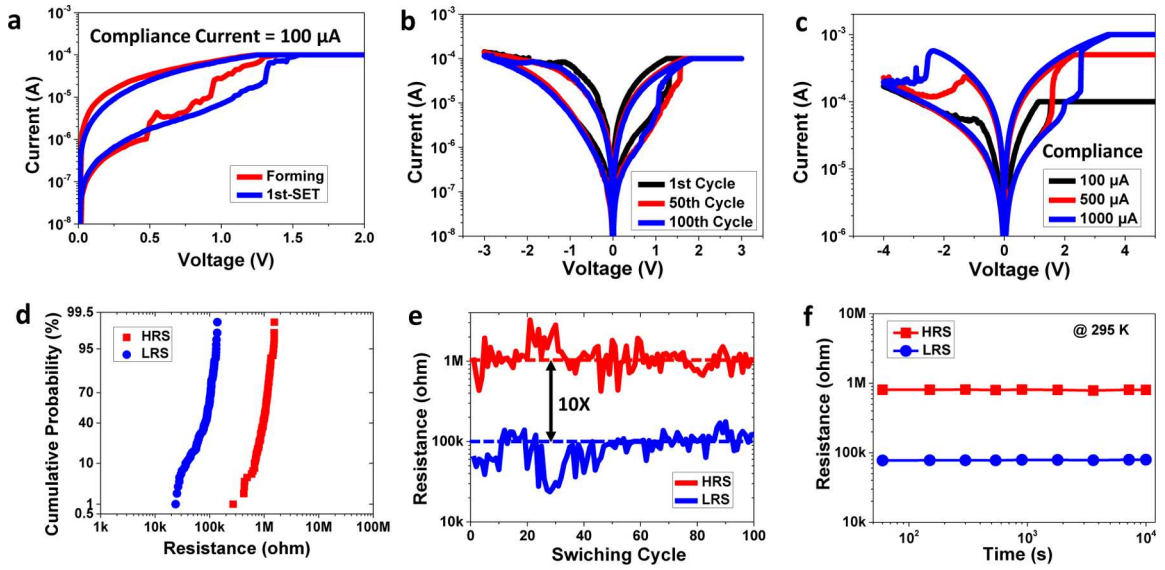

Figure 3. Electrical characterization of LSG-ReRAM. (a) Forming and first-SET curves indicate that the LSG-ReRAM is forming free. (b) Resistive switching behaviors of LSG-ReRAM at the first, 50th and 100th cycle, respectively. (c) Resistive switching behavior of the LSG-ReRAM under different current compliance, suggesting the potential of the multi-level cell application. (d) Distribution of HRS/LRS resistances obtained by dc sweep in LSG-ReRAM. (e) The dc switching endurance of LSG-ReRAM. (f) Retention measurement of LSG-ReRAM at room temperature.

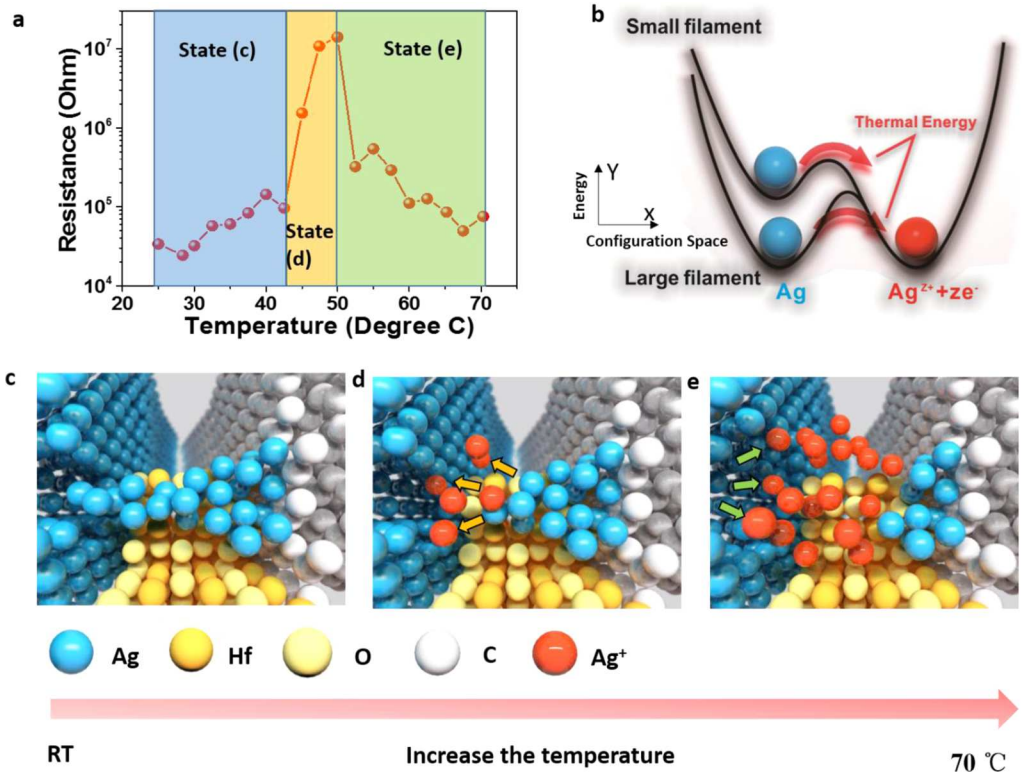

Figure 4. Temperature stability of the ON resistance. (a) Temperature stability test of the ON state of the LSG-ReRAM. The three regions represent the different states of the cell at the respective temperatures. The observed behavior is consistent with the previously reported temperature curves of cation-based ReRAM.[22] (b) Energy diagram showing a charge transfer reaction between an Ag atom in the filaments and an Ag ion dissolved in the HfO_x film. (c–e) Schematic diagrams showing the states in the device at the respective temperature. The orange arrow indicates the Ag^+ that comes from the original filament. The green arrow indicates the Ag^+ that comes from anode.

layer is almost transparent in the main SEM image. The thin layer of HfO_x coated on the graphene is more easily visible in the zoomed-in image (see top inset). Similarly, in the zoomed-in image, the stack of rGO layers could be identified as well (see bottom inset). The elements and distribution of Ag, Hf, C, O, and S in LSG-ReRAM are analyzed by EDS mapping (Figure S5).

Electrical Performance of the LSG-ReRAM. The effective cross-point area of the LSG-ReRAM is estimated to be 20 × 125 μm^2 (Figure S6). Since the LSG is 20 μm in width, the LSG wires

dx.doi.org/10.1021/nl5005916 | *Nano Lett.* 2014, 14, 3214–3219

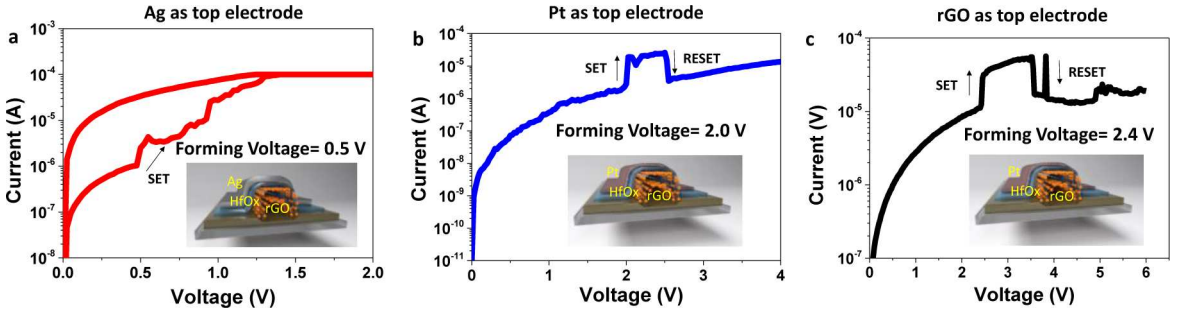

Figure 5. Memory forming characteristics of LSG-ReRAM under different top electrodes. Forming behavior with (a) Ag, (b) Pt, and (c) rGO as the top electrode.

could work as probe pads. The contact resistance between the LSG wires and the tungsten probe is examined to be 4605 Ω (Figure S7). Thus, the contact resistance should not impact on the electrical measurement results because it is ∼20 times lower than the low resistance state (LRS) of the LSG-RRAM. A single wire shown in Figure 2a functions as the bottom electrode of the LSG-RRAM. The LSG-ReRAM is forming-free using a 100 μA compliance current (Figure 3a). The SET process is considered to make the resistance of the ReRAM change from high to low. It is shown that the $I-V$ curves of the forming (first SET) and the second SET are very similar. The dc $I-V$ characteristics for the first, 50th and 100th cycle demonstrate that the LSG-ReRAM can be switched repeatedly (Figure 3b). In conventional cation-based ReRAM, the SET is abrupt.[17] However, the SET current increase is gradual in the LSG-ReRAM. The filament growth direction depends on the cation mobility in the oxide. Silver reportedly can act as a fast mobile ion in HfO_x.[26] As a result, the filament grows from the cathode to the anode.[26] It is speculated that when the Ag filament grows from rGO toward Ag, there may be a gap between the top of the filament and Ag anode, which could permit the flow of tunneling current. With the growth of the Ag filament toward Ag anode, the gap could become smaller and the tunneling current could become larger, causing the current to increase gradually instead of abruptly. The other possible reason for the gradual current increase during SET is that the initial Ag filament growth from graphene may be rather narrow. With the increase of the applied voltage, the filament could grow larger, which results in a gradual current increase. The ability to store 2-bit per memory cell is demonstrated using 100, 500, and 1000 μA compliance currents (Figure 3c). The resistance window is increased when the compliance current becomes larger due to the larger conduction filament width for a larger compliance current.[27] The distribution of the LRS and the high resistance state (HRS) is quite uniform with mean values of around 100 kΩ and 1 MΩ, respectively (Figure 3d). The dc endurance data of LSG-ReRAM is shown in Figure 3e where the HRS/LRS ratio is about 10. In general, HRS/LRS greater than or equal to 10 is preferred for practical memory application. Figure 3f shows the measured retention data of the LSG-ReRAM at room temperature. A retention time of up to 10^4 seconds (equal to ∼2.78 h) under 0.1 V reading voltage is achieved. Since the GO substrate is thermally sensitive, the retention measurement is not performed above room temperature. Further optimization of the endurance and the resistance window is necessary for practical applications.

Discussion. In order to determine whether the conducting filaments are formed from the Ag atoms or the oxygen vacancies, the resistance change of LSG-ReRAM is measured as a function of temperature. If the conducting filament is composed of Ag, the resistance is expected to increase at higher temperatures due to the increased electron scattering.[17] For oxygen-based ReRAM, the temperature dependence on resistance change is reported to be insignificant. For instance, less than 3% resistance change is expected within a temperature difference of 50 °C.[28] Figure 4a shows the change of LRS in the LSG-ReRAM when the temperature is gradually raised. Figure 4b shows schematic energy diagrams for Ag filaments and ions. The energy level for a small filament is higher than that for a large filament due to the higher surface energy. Since the Ag filaments can dissociate into Ag ions and electrons when there is enough thermal energy, the large filament could become smaller and may even break at the thinnest part at high temperatures. The plot of the LRS as a function of the temperature could be divided into three regions, which represent the three states, respectively. In state c, the filament is initially metallic, and the resistance gradually increases when the temperature goes higher. Such a phenomenon could be caused by two possible reasons. One is the increase of the electron scattering with temperature; the other comes from the reduction in diameter of the metal filament owing to the thermal dissolution.[29] As the temperature is being raised, two competing processes may happen simultaneously. The first is that the Ag filament dissolves into Ag^+ and this makes the filament become smaller and disconnected, thereby increasing the resistance of the device. The second is that the Ag anode dissolves into Ag^+ and makes the gap of the filament conductive, which can decrease the resistance of the device. At moderate temperatures, the former effect is dominant. It is speculated that the filaments dissolve and become smaller while the dissolution rate of Ag at the anode is relatively slower at that temperature. As a result, the resistance will increase with the temperature (illustrated in Figure 4d). When temperature is further increased, the second effect becomes dominant. The Ag^+ that dissolves from the Ag anode could make the gap conductive, and the resistance of the device decreases at a higher temperature (illustrated in Figure 4e). Next, a sudden resistance jump is observed in state d, which could be explained by the rupture of the Ag filaments. When the temperature increases, enough thermal energy could make Ag atoms in the thinnest part of the filament overcome the barrier and become Ag ions. Because of the concentration gradient, these Ag ions immediately diffuse into the surroundings, and the filament is disconnected at the thinnest part as illustrated in panel d of Figure 4. As a result, the measured resistance suddenly jumps to a high resistance state. After the filament is disconnected, a further temperature rise results in the gradual decrease in the on-resistance. It is speculated that in this regime, the concentration of Ag ions increase (Figure 4e) in the disconnected region due to thermal dissolution of the Ag anode and filament, which makes the filament gap conductive.[30]

dx.doi.org/10.1021/nl5005916 | *Nano Lett.* 2014, 14, 3214−3219

Control experiments are carried out to further investigate the switching mechanism. The forming behavior is an important indicator to tell the difference between cation-based ReRAM and oxide-based ReRAM. When a high electrical field is present in the oxide-based ReRAM, the oxygen ions will migrate toward to the interface of electrode/oxide and leave oxygen vacancies. The filament is formed by the connection of oxygen vacancies. Therefore, a high bias voltage is always required to form the filament.[23] Meanwhile, in cation-based ReRAM, the forming process represents the first formation of a metal filament based on solid electrochemical reactions. Hence, as long as the bias voltage is higher than the potentials needed for the anodic dissolution and cathodic deposition, then the memory cell can be SET even at a low applied bias voltage.[29] A higher SET voltage simply accelerates the time required for the formation of the conductive filament in an exponential voltage−time relationship.[31] The control experiments (Supporting Information, Figures S8 and S9) show that the GO or LSG do not serve as the resistive switching layer, which confirms that the HfO_x is required as a switching layer in the LSG-ReRAM.

As shown in Figure 5, the forming voltage of the device with Ag top electrode is just 0.5 V for the LSG-ReRAM, while the forming voltages of the devices with Pt and graphene as top electrodes are 2.0 and 2.4 V respectively. Therefore, the unipolar LSG-ReRAM with Pt as top electrode and rGO as bottom electrode might be related to oxide-based ReRAM, in which the HfO_x is electrically broken down to form oxygen vacancies. Moreover, the LSG-ReRAM with rGO as top electrode and Pt as bottom electrode also exhibit similar behaviors. The mechanism should be also relevant to the movement of oxygen ions. Memory switching using rGO as the top electrode is shown as Figure S10. Similar results using rGO as top electrodes were also reported by Yao et al.[24] In sum, there are several observations that lead to the conclusion that the LSG-ReRAM with Ag top electrode operates as a cation-based ReRAM: (i) The forming voltage is lower than the electrical breakdown voltage of HfO_x; (ii) the switching characteristic is bipolar, which is consistent with the previously reported cation-based ReRAM;[32] and (iii) the temperature-dependent resistance change behavior is observed to be similar to that reported for cation-based ReRAM.[29] The proposed switching mechanism of LSG-ReRAM is shown in Figure S11.

This work demonstrates an rGO-based memory fabricated by laser-scribing technology. As compared with metal electodes, rGO has shown several advantages. First, metal electrodes have a low flexibility. The rGO possesses a high stain tolerance, which is suitable as a flexible RRAM electrode. Second, metal electrodes such as Pt and Au are rare and costly while carbon-based materials are in abundance and the fabrication process of rGO is cost-efficient. Third, metal electrodes call for additional lithography or masks to define its shape. The rGO could be fabricated using the time-efficient laser-scribing technology without the use of masks. Finally, metal electrodes such as Cu might be easily oxidized in ambient conditions. Ruoff et al. demonstrated that Cu coated with graphene is able to protect the surface from air oxidation.[33] Thus, rGO is stable under ambient condition.

Laser-scribing technology now holds potential for making wafer-scale graphene-based systems that may comprise previously reported LSG components such as capacitors,[12] gas sensors,[13] strain sensors,[14] and transistors, photodetectors, and loudspeakers.[15] The whole graphene-based system could be made on a flexible substrate using laser-scribing technology. The present minimum resolution of the DVD laser scribing is 20 μm. In the future, higher resolution may be desired to achieve smaller memory cell sizes and improve the integration density of LSG-ReRAM arrays. The compatibility of laser-scribing technology with other conventional CMOS fabrication process needs to be further investigated for building more complex rGO-based systems. This laser-scribing technology may pave the way to facilitate graphene research towards the system level in the future.

Conclusion. In summary, a low-cost, transfer-free, flexible LSG-ReRAM is demonstrated for the first time. Using laser scribing enables the direct growth of rGO patterns on PET substrates. Electrical characterization of LSG-ReRAM devices show good resistance switching performance up to 100 cycles measured on the Ag/HfOx/LSG structure. In addition, the LSG-ReRAM exhibits forming-free character, reasonable reliability performance and 2-bit storage capability. Temperature dependence of the resistance change of LSG-ReRAM with Ag as the top electrode reveals that the conduction mechanism could be explained by cation filaments similar to a cation-based ReRAM. This work suggests that the laser scribing technology could realize rGO-based ReRAM and holds the potential for multifunctional rGO-based systems.

Method. *LSG Preparation.* A common Hummers method was used to synthesize a GO dispersion with a 2 mg/mL concentration using graphite powder provided by XFNANO Materials Tech Co., Ltd. (Nanjing, China).[34] About 10 mL GO solution was drop-casted on the surface of a LightScribe DVD disc. The GO solution was left overnight to dry on the DVD disc. After that, the GO coated DVD disc was patterned by the LightScribe DVD Drive (HP Inc. 557S). Using the Nero Start Smart software, the designed structure was transferred onto the GO film by the DVD laser-induced reduction of the GO into rGO.

LSG-ReRAM Fabrication Process. The first step was drop-casting a GO solution on the PET substrate coated on a DVD media disc. After the GO has dried, the whole disc was inserted into a LightScribe DVD drive. The 788 nm laser with a 5 mW maximum power inside the drive heats up the golden-brown GO and reduces it into black rGO at precise locations. Following this, 10 nm HfO_x was blanket deposited by thermal evaporation. Because the rGO would be further reduced under thermal treatment, subsequent fabrication steps with temperature greater than 100 °C should be avoided. On the basis of this consideration, the top electrode of LSG-ReRAM was made by curable silver paste at room temperature or using low temperature thermal evaporation. The top electrode could also be defined by photolithography.

Characterization of the LSG-ReRAM. The surface morphology of the LSG-ReRAM is observed using a Quanta FEG 450 SEM (FEI Inc.). The EDS mapping of the LSG-ReRAM is captured by the JSM-6301F SEM (JEOL Inc.). The Raman spectroscopy is obtained using a laser with a wavelength of 532 nm (HORIBA Inc.). The XPS is captured using EscaLab 250XI (Thermo Fisher Scientific Inc.). The electrical testing was done using a standard probe station (Agilent Inc. B1500).

■ ASSOCIATED CONTENT

Ⓢ Supporting Information

Testing results and discussion of LSG-ReRAM. This material is available free of charge via the Internet at http://pubs.acs.org.

■ AUTHOR INFORMATION

Corresponding Authors

*(T.-L.R.) E-mail: RenTL@tsinghua.edu.cn.

*(H.-S.P.W.) E-mail: hspwong@stanford.edu.

Author Contributions

†These authors contributed equally to this work.

Notes

The authors declare no competing financial interest.

■ ACKNOWLEDGMENTS

This work was supported by the National Natural Science Foundation of China (61025021, 60936002, 51072089, and 61020106006), the National Key Project of Science and Technology (2011ZX02403-002) and the Special Fund for Agro-scientific Research in the Public Interest (201303107). H.T. is additionally supported by the Ministry of Education Scholarship of China. This work was also supported by the Stanford School of Engineering China Ph.D. Research Exchange Program (H.-Y.C.), the member companies of Stanford Non-Volatile Memory Technology Research Initiative (NMTRI), Stanford Center for Integrated Systems, and STARnet SONIC. H.-Y.C. is additionally supported by Intel Fellowship and the Taiwanese Government Scholarship to Study Abroad (GSSA). M.A.M. is supported by the postdoctoral fellowship (PDF) program of the Natural Sciences and Engineering Research Council of Canada (NSERC).

■ REFERENCES

(1) Geim, A. K.; Novoselov, K. S. *Nat. Mater.* **2007**, *6*, 183−191.
(2) Novoselov, K.; Fal, V.; Colombo, L.; Gellert, P.; Schwab, M.; Kim, K. *Nature* **2012**, *490*, 192−200.
(3) Bae, S.; Kim, H.; Lee, Y.; Xu, X.; Park, J.-S.; Zheng, Y.; Balakrishnan, J.; Lei, T.; Kim, H. R.; Song, Y. I. *Nat. Nanotechnol.* **2010**, *5*, 574−578.
(4) Ryu, J.; Kim, Y.; Won, D.; Kim, N.; Park, J. S.; Lee, E. K.; Cho, D.; Cho, S. P.; Kim, S. J.; Ryu, G. H.; Shin, H. A. S.; Lee, Z.; Hong, B. H.; Cho, S. *ACS Nano* **2014**, *8*, 950−956.
(5) Gao, L.; Ni, G.-X.; Liu, Y.; Liu, B.; Neto, A. H. C.; Loh, K. P. *Nature* **2013**, *505*, 190−194.
(6) Lin, Y.-C.; Jin, C.; Lee, J.-C.; Jen, S.-F.; Suenaga, K.; Chiu, P.-W. *ACS Nano* **2011**, *5*, 2362−2368.
(7) Liang, X.; Sperling, B. A.; Calizo, I.; Cheng, G.; Hacker, C. A.; Zhang, Q.; Obeng, Y.; Yan, K.; Peng, H.; Li, Q. *ACS Nano* **2011**, *5*, 9144−9153.
(8) Wei, Z.; Wang, D.; Kim, S.; Kim, S.-Y.; Hu, Y.; Yakes, M. K.; Laracuente, A. R.; Dai, Z.; Marder, S. R.; Berger, C. *Science* **2010**, *328*, 1373−1376.
(9) Eda, G.; Fanchini, G.; Chhowalla, M. *Nat. Nanotechnol.* **2008**, *3*, 270−274.
(10) Robinson, J. T.; Zalalutdinov, M.; Baldwin, J. W.; Snow, E. S.; Wei, Z.; Sheehan, P.; Houston, B. H. *Nano Lett.* **2008**, *8*, 3441−3445.
(11) El-Kady, M. F.; Strong, V.; Dubin, S.; Kaner, R. B. *Science* **2012**, *335*, 1326−1330.
(12) El-Kady, M. F.; Kaner, R. B. *Nat. Commun.* **2013**, *4*, 1475.
(13) Strong, V.; Dubin, S.; El-Kady, M. F.; Lech, A.; Wang, Y.; Weiller, B. H.; Kaner, R. B. *ACS Nano* **2012**, *6*, 1395−1403.
(14) Tian, H.; Shu, Y.; Cui, Y.-L.; Mi, W.-T.; Yang, Y.; Xie, D.; Ren, T.-L. *Nanoscale* **2013**, *6*, 699−705.
(15) Tian, H.; Yang, Y.; Xie, D.; Cui, Y.-L.; Mi, W.-T.; Zhang, Y.; Ren, T.-L. *Sci. Rep.* **2014**, *4*, 3598.
(16) Waser, R. *Microelectron. Eng.* **2009**, *86*, 1925−1928.
(17) Kund, M.; Beitel, G.; Pinnow, C.-U.; Rohr, T.; Schumann, J.; Symanczyk, R.; Ufert, K.-D.; Muller, G. *IEEE Int. Electron Devices Meet.* **2005**, 754−757.
(18) Wong, H.-S.; Lee, H.-Y.; Yu, S.; Chen, Y.-S.; Wu, Y.; Chen, P.-S.; Lee, B.; Chen, F. T.; Tsai, M.-J. *Proc. IEEE* **2012**, *100*, 1951−1970.
(19) Govoreanu, B.; Kar, G.; Chen, Y.; Paraschiv, V.; Kubicek, S.; Fantini, A.; Radu, I.; Goux, L.; Clima, S.; Degraeve, R. *IEEE Int. Electron Devices Meet.* **2011**, 31.6. 1−31.6. 4.
(20) Chen, H.-Y.; Yu, S.; Gao, B.; Huang, P.; Kang, J.; Wong, H.-S. P. *IEEE Int. Electron Devices Meet.* **2012**, 20.7. 1−20.7. 4.
(21) Lee, M.-J.; Lee, C.; Kim, S.; Yin, H.; Park, J.; Ahn, S.; Kang, B.; Kim, K.; Stefanovich, G.; Song, I. *IEEE Int. Electron Devices Meet.* **2008**, 1−4.
(22) Hong, A. J.; Song, E. B.; Yu, H. S.; Allen, M. J.; Kim, J.; Fowler, J. D.; Wassei, J. K.; Park, Y.; Wang, Y.; Zou, J. *ACS Nano* **2011**, *5*, 7812−7817.
(23) Tian, H.; Chen, H.-Y.; Gao, B.; Yu, S.; Liang, J.; Yang, Y.; Xie, D.; Kang, J.; Ren, T.-L.; Zhang, Y. *Nano Lett.* **2013**, *13*, 651−657.
(24) Yao, J.; Lin, J.; Dai, Y.; Ruan, G.; Yan, Z.; Li, L.; Zhong, L.; Natelson, D.; Tour, J. M. *Nat. Commun.* **2012**, *3*, 1101.
(25) Chen, H.-Y.; Tian, H.; Gao, B.; Yu, S.; Liang, J.; Kang, J.; Zhang, Y.; Ren, T.-L.; Wong, H.-S. P. *IEEE Int. Electron Devices Meet.* **2012**, 20.5. 1−20.5. 4.
(26) Haemori, M.; Nagata, T.; Chikyow, T. *Appl. Phys. Express* **2009**, *2*, 1401.
(27) Russo, U.; Kamalanathan, D.; Ielmini, D.; Lacaita, A. L.; Kozicki, M. N. *IEEE Trans. Electron Devices* **2009**, *56*, 1040−1047.
(28) Miao, F.; Strachan, J. P.; Yang, J. J.; Zhang, M. X.; Goldfarb, I.; Torrezan, A. C.; Eschbach, P.; Kelley, R. D.; Medeiros-Ribeiro, G.; Williams, R. S. *Adv. Mater.* **2011**, *23*, 5633−5640.
(29) Tsuruoka, T.; Terabe, K.; Hasegawa, T.; Aono, M. *Nanotechnology* **2010**, *21*, 425205.
(30) Guan, W.; Liu, M.; Long, S.; Liu, Q.; Wang, W. *Appl. Phys. Lett.* **2008**, *93*, 223506.
(31) Yu, S.; Wong, H.-S. *IEEE Trans. Electron Devices* **2011**, *58*, 1352−1360.
(32) Li, Y.; Long, S.; Lv, H.; Liu, Q.; Wang, Y.; Zhang, S.; Lian, W.; Wang, M.; Zhang, K.; Xie, H. *Nanotechnology* **2011**, *22*, 254028.
(33) Chen, S.; Brown, L.; Levendorf, M.; Cai, W.; Ju, S.-Y.; Edgeworth, J.; Li, X.; Magnuson, C. W.; Velamakanni, A.; Piner, R. D. *ACS Nano* **2011**, *5*, 1321−1327.
(34) Hummers, W. S., Jr.; Offeman, R. E. *J. Am. Chem. Soc.* **1958**, *80*, 1339−1339.